ELSEVIER

PII: S0032-3861(98)00093-7

Polymer Vol. 39 No. 26, pp. 6733–6742, 1998
© 1998 Elsevier Science Ltd
Printed in Great Britain. All rights reserved
0032-3861/98/$ - see front matter

Is the Maxwell–Sillars–Wagner model reliable for describing the dielectric properties of a core–shell particle–epoxy system?

B. Lestriez[a,*], A. Maazouz[a], J. F. Gerard[a], H. Sautereau[a], G. Boiteux[b], G. Seytre[b] and David E. Kranbuehl[c]

[a]*Laboratoire des Materiaux Macromoleculaires, UMR 5627, INSA Lyon, Bat. 403, 20 av. A. Einstein, 69621 Villeurbanne, France*

[b]*Laboratoire d'Etudes des Materiaux Plastiques et Biomateriaux, UMR 5627, Universite 'Claude Bernard', 43 bv du 11 Nov 1918, 69622 Villeurbanne, France*

[c]*Chemistry Department, College of William and Mary, Williamsburg, VA 23187, USA*

(Received 4 November 1997; accepted 9 December 1997)

Dielectric measurements have been performed on neat acrylic core–shell particles, and core–shell modified-epoxy networks in order to assess the accuracy of the Maxwell–Wagner–Sillars (MWS) model in describing the dielectric properties of heterogeneous polymeric systems. Measured and predicted interfacial polarizations are compared. The temperature dependence of the frequency of maximum interfacial dielectric loss process is well described by the MWS model and from the temperature dependence of the conductivity of the two phases. However, the measured and predicted absolute values differ and a distribution in the interfacial relaxation time is observed. This is attributed to the effect of a gradient in concentration across the interface between the acrylic particles and the epoxy matrix. It is thus concluded that the nature and properties of interphases can strongly influence the dielectrical properties and interfacial polarization processes in polymer blends, and that theoretical models which do not take into account details of interfacial charge transfer might not be reliable in describing the morphology of heterogeneous polymeric systems. © 1998 Elsevier Science Ltd. All rights reserved.

(Keywords: dielectric properties; polymer blends; interfacial polarization)

INTRODUCTION

Over the past two decades time dependent dielectric measurements made over many decades in frequency have become an effective in-situ instrumental means of observing the changing physical properties of a polymer resin during polymerization. Due to the development of micro-sensors, dielectric techniques have been adapted for use both in the laboratory and in industrial manufacturing–processing environments. These dielectric techniques have found a use in characterizing the viscosity changes and the degree of cure, i.e. T_g, during polycondensation[1–10].

In recent years, a major emphasis of high performance polymer research has focused on the development of two-phase thermoplastic/thermoset systems to improve upon thermoset embrittlement and to obtain an optimum combination of properties involving the toughness of thermoplastics and the processability, strength and durability of thermosets. Important to the development of such materials is the ability to observe the phase separation process and to characterize the two-phase morphology. Over the past 5 years, a number of authors have used dielectric measurements to characterize the development of the two-phase morphology in toughened thermosets[11–17] by considering the Maxwell–Wagner–Sillers model for analyzing their dielectric measurements. In each of these cases numerous approximations and assumptions must be made regarding structure, shape and orientation of the embedded particles, in addition to approximate estimation of the dielectric properties and composition of the two phases resulting from the phase separation process. Further, aside from a number of classical papers on metal, mineral and water conductive occlusions in nonconducting media (see Refs 18,19 and references therein), there are few papers which focus on the ability of this widely used model to accurately describe the dielectric properties in polymeric two-phase systems.

The aim of this paper is to assess the accuracy of the Maxwell–Wagner–Sillars (MWS) model. Acrylic core–shell particles having a well-defined shape are dispersed in an epoxy matrix. As a consequence, in this case, the dielectric properties of the particles and the matrix are well-known whereas these properties cannot be known in systems generated from a phase separation phenomena. Thus dielectric measurements have been performed on the core–shell particles of defined and uniform geometry, on the neat epoxy matrix and on the two-phase blend. The measured dielectric properties are then compared with the predictions of the MWS model.

THEORETICAL AND BACKGROUND

Interfacial polarization processes occur in heterogeneous dielectrics as a result of the build-up of space charges at interfaces between two media having differing permittivities and conductivities[20].

Van Beek and Bánhegyi reviewed the different models which can be used to calculate the dielectric properties of heterogeneous materials on the basis of the dielectric

* To whom correspondence should be addressed

properties of the components, the volume fraction and the geometry of the phases[18–20].

The formulae are divided into two subgroups: asymmetric (matrix inclusion type) and symmetric (statistical mixture type) equations.

Among the former group, one distinguishes at low volume fraction the well-known Maxwell–Sillars–Wagner model[21–23]. The complex dielectric permittivity of the mixture $\varepsilon^*(\omega)$ of orientated ellipsoids with complex dielectric constant, $\varepsilon_2^*(\omega)$, at a volume fraction ν_2 dispersed in a continuous matrix with a complex dielectric constant, $\varepsilon_1^*(\omega)$, can be calculated from the following equation:

$$\varepsilon^* = \varepsilon_1^* \frac{\varepsilon_1^*(1-\nu_2)(1-A) + \varepsilon_2^*(\nu_2 + A(1-\nu_2))}{\varepsilon_1^* + A(1-\nu_2)(\varepsilon_2^* - \varepsilon_1^*)} \quad (1)$$

where A ($0 \leq A \leq 1$), is the depolarization factor of the ellipsoidal filler particles. It depends on the shape of the particles (length of the long a to b short axis ratio for spheroids) and the orientation of the field relative to the particle. For prolate spheroids (rod or needle-like) oriented along their larger axis, A lies between 0 and 1/3, while for oblate spheroids (disc-like) oriented along the shorter axis, A lies between 1/3 and 1; $A = 1/3$ in the case of spheres. Separating the real and imaginary parts leads to Debye's equations

$$\varepsilon' = \varepsilon_\infty + \frac{\varepsilon_s - \varepsilon_\infty}{1 + (\omega\tau_{\mathrm{MWS}})^2} \quad (2)$$

$$\varepsilon'' = (\varepsilon_s - \varepsilon_\infty)\frac{\omega\tau_{\mathrm{MWS}}}{1 + (\omega\tau_{\mathrm{MWS}})^2} \quad (3)$$

where ω is the angular frequency, with explicit formulae for the low and high frequency limiting permittivity ε_s, ε_∞ and τ_{MWS} the relaxation time of the interfacial polarization.

$$\tau_{\mathrm{MWS}} = \varepsilon_0 \frac{\varepsilon_1 + A(1-\nu_2)(\varepsilon_2 - \varepsilon_1)}{\sigma_1 + A(1-\nu_2)(\sigma_2 - \sigma_1)} \quad (4)$$

$$\varepsilon_s = \varepsilon_1 \frac{\sigma_1 + [A(1-\nu_2) + \nu_2](\sigma_2 - \sigma_1)}{\sigma_1 + A(1-\nu_2)(\sigma_2 - \sigma_1)} + \nu_2\sigma_1 \frac{[\sigma_1 + A(\sigma_2 - \sigma_1)](\varepsilon_2 - \varepsilon_1) - [\varepsilon_1 + A(\varepsilon_2 - \varepsilon_1)](\sigma_2 - \sigma_1)}{[\sigma_1 + A(1-\nu_2)(\sigma_2 - \sigma_1)]^2} \quad (5)$$

$$\varepsilon_\infty = \varepsilon_1 \frac{\varepsilon_1 + [A(1-\nu_2) + \nu_2](\varepsilon_2 - \varepsilon_1)}{\varepsilon_1 + A(1-\nu_2)(\varepsilon_2 - \varepsilon_1)} \quad (6)$$

where ε_0 denotes permittivity of free space, σ_1, σ_2, ε_1 and ε_2 are the conductivities and limiting permittivities (for which by definition $\varepsilon'' = 0$) of the matrix (index 1) and the occluded phase (index 2). Fricke[24] extended the MWS model to randomly orientated ellipsoids. Equations (2)–(6) show that in such a case a distribution in the morphology (shape and/or orientation) of the occluded ellipsoids leads to a distribution of the relaxation times because of the distribution of the A values.

When the concentration of particles in the immediate neighbourhood of a given particle is considered for high volume fraction, Bruggeman–Hanaï[25], Boyle[26] and Boned–Peyrelasse[27] obtained formulae for spheres, orientated and randomly orientated ellipsoids dispersed in an effective medium whose dielectric properties are that of the mixture. No equations can be derived for a relaxation time and Debye equations cannot be applied.

More recently, Steeman and Maurer[28,29] derived an interlayer model for the complex dielectric constant of ellipsoidally shaped particles surrounded by an interlayer and dispersed into a matrix. When the volume fraction of the interface layer equals zero, this model reduces to the MWS model. In the case of nonconductive filler covered by a very thin conductive layer embedded into an insulating matrix, the Steeman–Maurer model reduces to a Debye-type dispersion in which:

$$\tau = \left(\frac{\nu_{\mathrm{core}}}{1-\nu_{\mathrm{core}}}\right)\left(\frac{3\varepsilon_0}{2\sigma_{\mathrm{shell}}\nu_{\mathrm{shell}}}\right)\left[\left(\varepsilon_{\mathrm{core}} + 2\varepsilon_{\mathrm{matrix}}\right) - \left(\varepsilon_{\mathrm{core}} - \varepsilon_{\mathrm{matrix}}\right)\nu_{\mathrm{core}}\right] \quad (7)$$

$$\varepsilon_s = \left(\frac{1+2\nu_{\mathrm{core}}}{1-\nu_{\mathrm{core}}}\right) \quad (8)$$

$$\varepsilon_\infty = \frac{(\varepsilon_{\mathrm{core}} + 2\varepsilon_{\mathrm{matrix}}) + 2(\varepsilon_{\mathrm{core}} - \varepsilon_{\mathrm{matrix}})\nu_{\mathrm{core}}}{(\varepsilon_{\mathrm{core}} + 2\varepsilon_{\mathrm{matrix}}) - (\varepsilon_{\mathrm{core}} - \varepsilon_{\mathrm{matrix}})\nu_{\mathrm{core}}} \quad (9)$$

Each of these matrix inclusion type equations predict strong interfacial loss only if the more conducting component is the inclusion phase. The static conductivity is theoretically governed by that from the matrix phase.

When no clear assignment of a matrix component and a filler component can be made, symmetrical mixture type equations are considered. Both components are considered to be embedded in an effective medium with properties of the mixture. The Looyenga[30], equation (10), and Brüggeman–Böttcher–Hsu[31,32] formulae are obtained

$$(\varepsilon^*)^{1-2A} = \nu_1(\varepsilon_1^*)^{1-2A} + \nu_2(\varepsilon_2^*)^{1-2A} \quad (10)$$

If only one component is conductive, the Brüggeman–Böttcher–Hsu[31,32] equation predicts a percolation threshold while the Looyenga equation predicts conduction for $A < 0.5$ in the whole composition range. No equations can be derived for a relaxation time and Debye equations cannot be applied.

According to Bánhegyi[20], matrix inclusion type equations are suitable for the description of emulsions and filled polymers if none of the components exhibits metallic conductivity. Statistical mixture formulae are suitable for compacted powders, interpenetrating network structures and heterogeneous polymer mixtures. All of these equations are based on continuum electrodynamic equations. They do not take into account the mechanism of conduction nor the details of interfacial charge transfer.

Low frequency effects are often mentioned in heterogeneous systems and attributed to interfacial polarization[33–43]. Only a few quantitative descriptions of the detected effects based on the equations previously mentioned have been given. Matrix inclusion formulae were in good agreement with the experimental data for polycarbonate/styrene–acrylonitrile copolymer multilayers structures[33] and clay-filled ethylene–propylene rubber copolymer[44]. For glass-bead reinforced polystyrene[45] the interfacial relaxation time was predicted to be within 10% of the MWS model prediction up to a volume fraction of 0.20. At higher content, the model diverged. Phase separated systems like epoxy–elastomer[14–16] or epoxy–thermoplastic[12,13] blends seem to obey these matrix inclusive laws as an interfacial polarization effect is only detected if the conductive phase (elastomer for the first case and epoxy for the second) is the occluded one. On the other hand, Steeman[46] showed that the

interfacial loss detected on a polycarbonate/styrene-*co*-acrylonitrile containing a butadiene rubber blend was much better described by the Looyenga statistical mixture equation.

Theoretical results from Boned and Peyrelasse[27] show that matrix inclusion type heterogeneous materials should display symmetrical relaxation (circular arc with centre lying below the horizontal axis on a Cole–Cole plot) only in the case of dispersed spheres. The asymmetry of the interfacial polarization (skewed arcs on a Cole–Cole plot) should increase with increasing a/b asymmetry of the ellipsoid. Hollow glass-bead triazine-based thermoset composites[47], clay-filled ethylene–propylene rubber copolymer ($a/b \leq 3$)[44], occluded spherical particles of amine-terminated polyoxypropylene or carboxyl-terminated poly(butadiene-*co*-acrylonitrile in an epoxy–amine cross-linked matrix[15,16] and poorly interdiffused PVC particles[48] gave rise to a symmetrical interfacial relaxation. An exception was reported by Perrier[45]. Glass beads dispersed in PS lead to a perfect Debye-like process for a volume fraction of 6.8%, while for 12.5–47.3%, asymmetrical relaxations were observed. Reducing the bead diameter from 90 to 20 μm resulted in a Debye-like MWS process up to a volume fraction of 20%.

According to the MWS model, an activation energy identical to the Arrhenius temperature dependence of the conductivity of the highly conductive components is to be expected. For small ν_2, and $\sigma_1 \ll A\sigma_2$, equation (4) can be reduced to:

$$\tau_{\mathrm{MWS}} = \varepsilon_0 \frac{[\varepsilon_1 + A(\varepsilon_2 - \varepsilon_1)]}{A\sigma_2} \tag{11}$$

As stressed by Aldrich[47]:

$$\frac{\partial(\ln \tau_{\mathrm{MWS}})}{\partial(1/T)} = \frac{-\partial(\ln \sigma_2)}{\partial(1/T)} + \frac{\partial(\ln[\varepsilon_1 + A(\varepsilon_2 - \varepsilon_1)])}{\partial(1/T)} \tag{12}$$

and in most polymeric systems, the second term of the right part of equation (12) is negligible. This correlation between τ_{MWS} and σ_2 has been observed experimentally[33,48]. Other studies showed an Arrhenius temperature dependence of the relaxation times[15,16].

EXPERIMENTAL

Materials

A mixture of diglycidylether of bisphenol-A (DGEBA, $M_n = 380$ g mol^{-1}) and 3 aminomethyl-3,5,5 trimethylcyclohexylamine (IPD, $M = 170$ g mol^{-1}) was used as the epoxy continuous phase. An amino hydrogen-to-epoxy ratio of 1 was chosen in order to obtain the higher glass transition temperature, T_g. A cure schedule of 1 h at 140°C followed by 6 h at 190°C was used. An industrial dried core–shell latex based on poly(butyl-acrylate) core ($T_g = -56$°C) and a carboxyl-functionalized cross-linked poly(methyl methacrylate) shell ($T_g = 95$°C) particle, denoted CSR1 (EXL 8666 from Rohm and Haas) was used as the dispersed phase. The mean diameter of the CSR1 particles is equal to 250 nm. The poly(methyl methacrylate) is 16% of the total mass, which means that the shell thickness may be greater or less than 7 nm according to the grafting density and the molecular weight of the poly(methyl methacrylate) chains[49]. The reagents and core–shell particles are described in *Table 1*. Measurements were also carried out on other core–shell particles denoted CSR2, which differ from the ones previously mentioned by their polybutadiene core (EXL 2611 from Rohm and Haas), and on a conventional poly(methyl methacrylate) ($M_w = 120.000$ and $I_p = 2.4$ from Aldrich).

A volume fraction of CSR1-particles equal to 15.3% was considered. The mixing of the DGEBA prepolymer and the CSR1 particles (dried for 2 h under vacuum at 80°C before use) was carried out under high speed mechanical stirring using a Ultraturax T50 device operating up to 8000 rpm. The temperature was kept below 90°C to prevent degradation of the shell. The comonomer IPD was added to the mixture under stirring. Trapped air was removed over 1 h under vacuum. The materials were moulded into 0.6 mm thick plates. The CSR1 and CSR2 particles were also moulded as 0.6 mm thick films by compression-moulding from the dried latex powders. They were obtained under different pressures (60, 100 and 150 bar) at 180°C.

The glass transition temperatures were measured using differential scanning calorimetry with a DSC7 Perkin Elmer apparatus under nitrogen atmosphere with a heating rate of 10°K min^{-1}. The morphology of the CSR1 and CSR2 films, and modified epoxy network was checked by transmission electron microscopy (TEM). In addition, dynamic mechanical spectroscopy was performed on a 2 mm thick CSR-film using a RDA700 viscoelasticimeter from Rheometrics operating at 1.6×10^{-2} and 10 Hz.

For electrical measurements, aluminium electrodes with a diameter of 20 mm were sputtered on both sides of the samples. They were then stored in a vacuum desiccator under the presence of silica gels. In any case, measurements were carried out under nitrogen atmosphere. Samples were first heated 20°C above T_g for 10 min to allow frozen-in deformation to relax and to ensure good contact with the electrodes.

DC conductivity measurements

Conductivity measurements were carried out in a two-electrode cell. The measuring circuit consisted of a Keithley 617 electrometer with incorporated voltage source, a PC computer for data acquisition, storage and handling of the results and the thermoregulated measurement oven. Measurements were performed on temperature steps (10 K interval). The cell was equilibrated for 35 min at the measurement temperature. A constant step voltage 100 V with a duration of 10 min was applied to the sample after which the measured resistance was used to calculate the DC conductivity. Between two measurements, the cell was short-circuited for 45 min.

Dielectric measurements

Dielectric measurements were performed on a dielectric thermal analyzer DEA 2970 from TA Instruments. Two types of experiment were carried out: isochronal runs at 2 K min^{-1} over a frequency range from 1 to 50 000 Hz (15 data points being collected within a period of 1 min) and isothermal runs at 10 K measurement intervals (26 data points were collected within a period of 10 min). The frequency range was from 0.01 to 50 000 Hz. The sample was kept for 45 min at each measurement temperature, 10 min being necessary to obtain thermal equilibrium. Each data point presented is an average of three values.

RESULTS

As shown in the TEM micrographs (*Figure 1*) the core–shell particles kept their morphology for compression-moulded dried latex (*Figure 1a*) and as a dispersed phase in the epoxy matrix (*Figure 1b*). The dynamic mechanical

Table 1 Reagents and components used to prepare the core–shell modified epoxies

Name	Chemical formula	Supplier
DGEBA	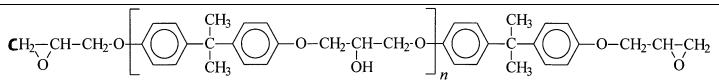 n = 0.15	Bakelite 0164
IPD	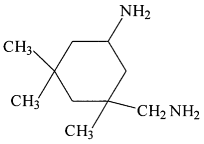	RX chimie
Core–shell	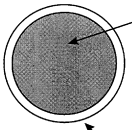 Core: CSR1 - Poly(butyl acrylate) (1) CSR2 - Polybutadiene (2) Shell :COOH-functionalized crosslinked poly(methyl methacrylate)	Rohm & Haas (1) EXL 8866 (2) EXL 2611

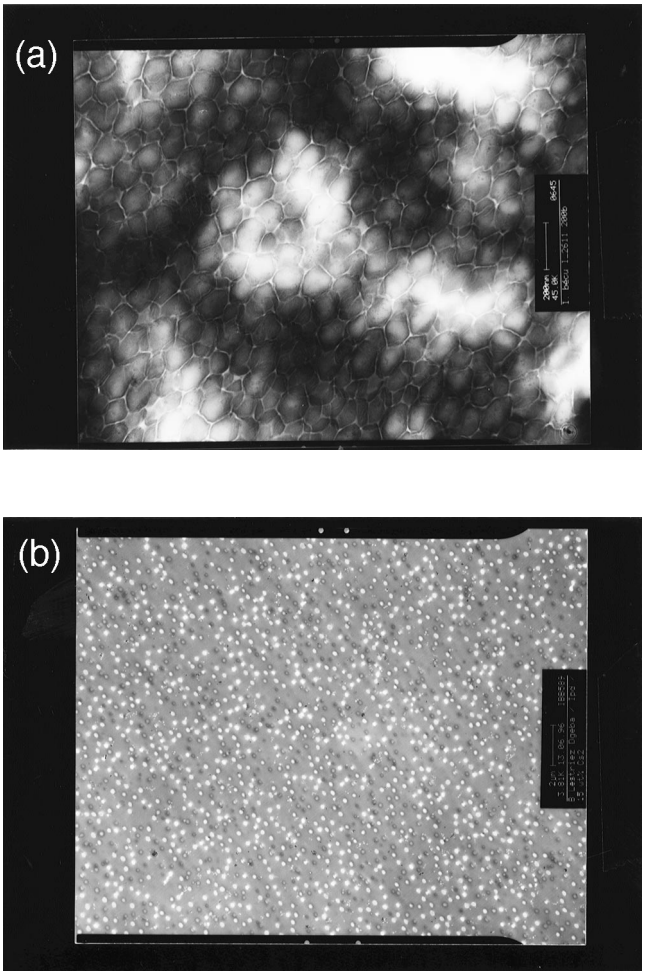

Figure 1 (a) TEM micrographs of the CSR2 film. (b) TEM micrograph of the CSR1-modified epoxy network (15.3% vol.)

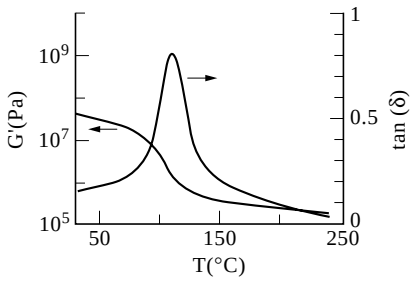

Figure 2 Dynamic mechanical spectra (G' and tan δ *versus* temperature) at 10 Hz of the CSR1 film (2 mm thick)

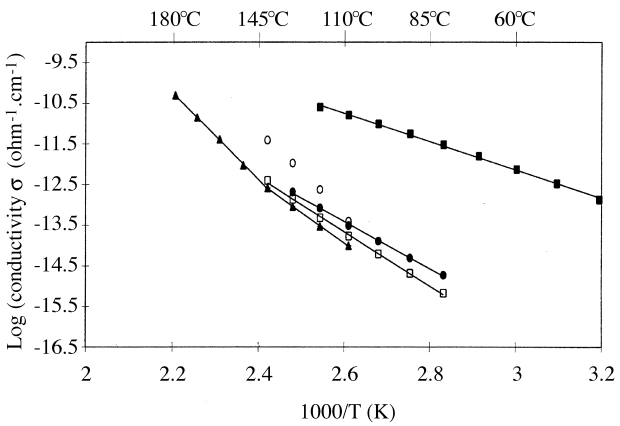

Figure 3 Log (conductivity) *versus* 1000/temperature for neat epoxy (▲), CSR1-modified epoxy system (●), CSR1 film (■), CSR2 film (□) and PMMA (○)

spectra of CSR1 particles show the main relaxation associated with the glass transition of the PMMA shell (*Figure 2*). The existence of a rubbery plateau indicates that the PMMA shell is cross-linked and that the processing (temperature, pressure) does not affect the core–shell particle structure. In addition *Figure 1b* shows that a good state of dispersion of the CSR1 particles within the epoxy was obtained.

During the emulsion polymerization of the CSR particles, the sodium dodecyl sulfate was used as emulsifier. After drying, it can be supposed that some of the surfactant remains adsorbed on the particle surface. Differential scanning calorimetry doesn't display a melting peak at 207°C of the sodium dodecylsulfate indicating that the commercial core–shell particles considered in this study were washed to remove the free stabilizer. Thus, the remaining surfactant should be strongly adsorbed on the particle's surface.

The measured glass transition temperature of the neat

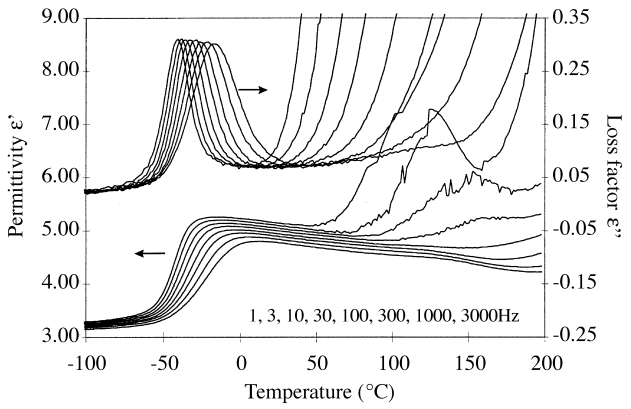

Figure 4 The dielectric constant ε' and loss factor ε'' of CSR1 film as a function of temperature at several frequencies

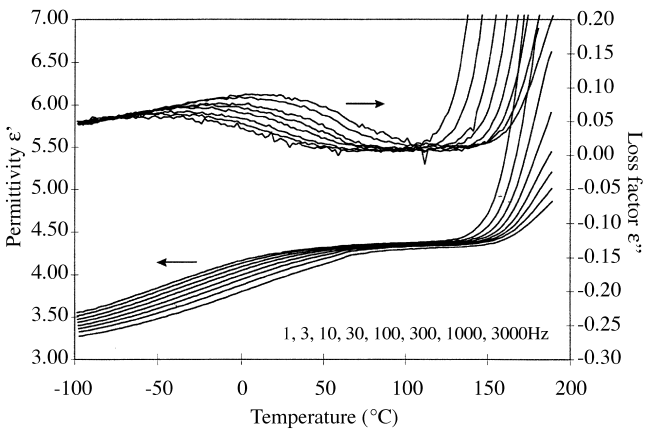

Figure 5 The dielectric constant ε' and loss factor ε'' of the neat epoxy network as a function of temperature at several frequencies

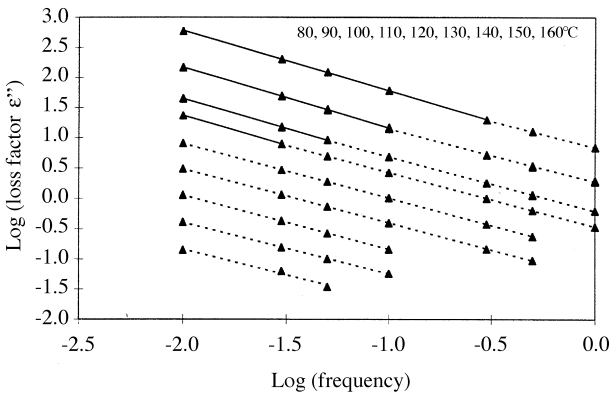

Figure 6 Log (loss factor ε'') *versus* log (frequency) at several temperatures for neat epoxy network (dashed lines for slope = 0.9 and full lines for slope = 1)

epoxy and modified-epoxy cured systems are 151 and 146°C, respectively. This slight decrease of T_g observed will not affect the electrical properties. It could be due to the overlapping of the glass transition region of the PMMA shell with that of the epoxy matrix.

Plots of log(conductivity) *versus* 1000/temperature are shown in *Figure 3* for the unmodified epoxy network, the CSR1 films and the modified epoxy network. Straight lines are obtained, indicating the presence of Arrhenius processes being thermally activated. Between 140 and 150°C, i.e. at the glass–rubber transition, the DC conductivity of the neat epoxy network rises due to an increase in the charge carriers' mobility. No difference in the DC conductivity of the CSR1 films was observed in relation to the compression-moulding conditions indicating the absence of air lamellae. Unexpectedly, no rise in the DC conductivity is observed above the glass transition temperature of the shell. An increase in the conductivity of the epoxy matrix is observed from the neat network to the CSR1-modified epoxy network. This increase is thought to be due to diffusion of sodium dodecyl sulfate surfactant from the shell surface into the epoxy matrix. Measurements carried out on CSR2 particles and on poly(methyl methacrylate) are also reported. They are examined in Section 5.

The permittivity, ε', and the loss factor, ε'', of the CSR1 films for frequencies from 1 to 3000 Hz as a function of temperature are shown in *Figure 4*. No difference was observed with varying moulding pressure. The loss factor displays a maximum due to the glass–rubber transition of the poly(butyl-acrylate) while in the same temperature range the dielectric constant increases from 3.2 to 5. With increasing frequency the transition is located at higher temperatures. Above the glass–rubber transition of the core the loss factor, ε'', displays a sharp increase due to electrical conduction of this medium. Simultaneously the permittivity, ε', at the low frequencies goes up to very high values which indicates an electrode polarization phenomena. The high frequencies reveal a relaxation associated with the glass–rubber transition of the shell.

The permittivity, ε', and the loss factor, ε'', of the unmodified epoxy network for frequencies from 1 to 3000 Hz as a function of temperature are shown *Figure 5*. At low temperature, the β peak is attributed to the relaxation of the hydroxyether units $-O-CH_2-CH(OH)-CH_2$ created during the cross-linking reactions and from the initial epoxy prepolymer[50]. In the high temperature region an electrode polarization phenomena leads to very high ε' values as a consequence of the rise in the conductivity as the glass–rubber transition is approached.

The measured loss index spectrum contains contributions from two sources: dipolar reorientation and diffusion of charge carriers. When interfacial polarization also occurs, it can be written,

$$\varepsilon''_{\mathrm{meas}}(\omega, T) = \varepsilon''_{\mathrm{pol}}(\omega, T) + \varepsilon''_{\mathrm{inter}}(\omega, T) + \varepsilon''_{\mathrm{DC}}(\omega, T) \quad (13)$$

with

$$\varepsilon''_{\mathrm{DC}}(\omega, T) = \sigma_{\mathrm{DC}}(T)/(\varepsilon_0 \omega^{1-k}) \quad (14)$$

where $0 \leq k \leq 1$. When the losses due to ohmic electrical conduction, $\varepsilon''_{\mathrm{DC}}$, dominates:

$$\varepsilon''_{\mathrm{meas}}(\omega, T) \approx \sigma_{\mathrm{DC}}(T)/(\varepsilon_0 \omega^{1-k}) \quad (15)$$

In *Figure 6* the logarithm$_{10}$ of the measured dielectric loss index, ε'', is plotted as a function of frequency at several temperatures between 80 and 150°C for the unmodified epoxy network. Two distinct dependencies with the frequency appear as the temperature reaches the highest values. Below a critical temperature dependent frequency, a mean 0.90 ± -0.01 value is obtained for the parameter $|1 - k|$. Above this critical temperature dependent frequency a mean 1.00 ± 0.01 value is found (all correlation parameters are > 0.999). We suspect the difference arises as a consequence of the electrode polarization phenomena observed on the lower frequencies. Between 80 and 120°C the CSR1 film displayed a $|1 - k|$ equal to 1.00 ± 0.01.

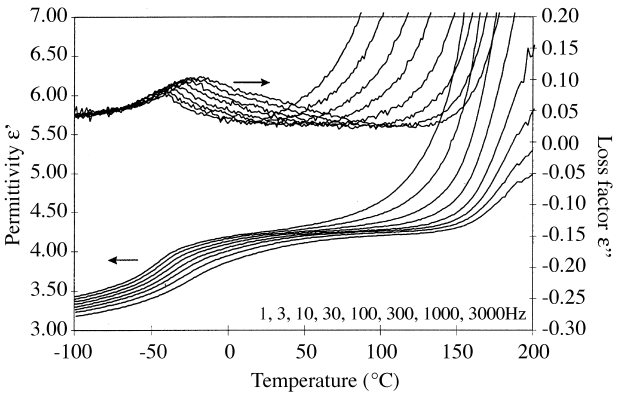

Figure 7 The dielectric constant ε' and loss factor ε'' of CSR1-modified epoxy network as a function of temperature at several frequencies

The dielectric spectrum of the modified epoxy network is shown in *Figure 7*. Between −50 and 50°C, the α relaxation of the core and β relaxation of the matrix superimpose. In comparison with the dielectric spectrum of the neat matrix (*Figure 5*), in the lowest frequency range a new process appears at 50°C. A higher level of conductivity is also found as observed with a large increase in the dielectric loss in the high temperature region. To study this process, isothermal measurements were carried out as described in the Experimental section. The permittivity, ε', (*Figure 8a*) and the loss factor, ε'', (*Figure 8b*) of the CSR1 film, the unmodified and modified epoxy system are shown at 100°C. A relaxation, which is not evidenced for the neat epoxy network is clearly displayed. In order to separate this expected MWS loss from the low frequency contribution of DC conductivity, it was necessary to subtract a contribution which is $1/\omega^{0.9}$ dependent. The $|1-k|$ parameter was found unchanged from the unmodified to the CSR1 modified

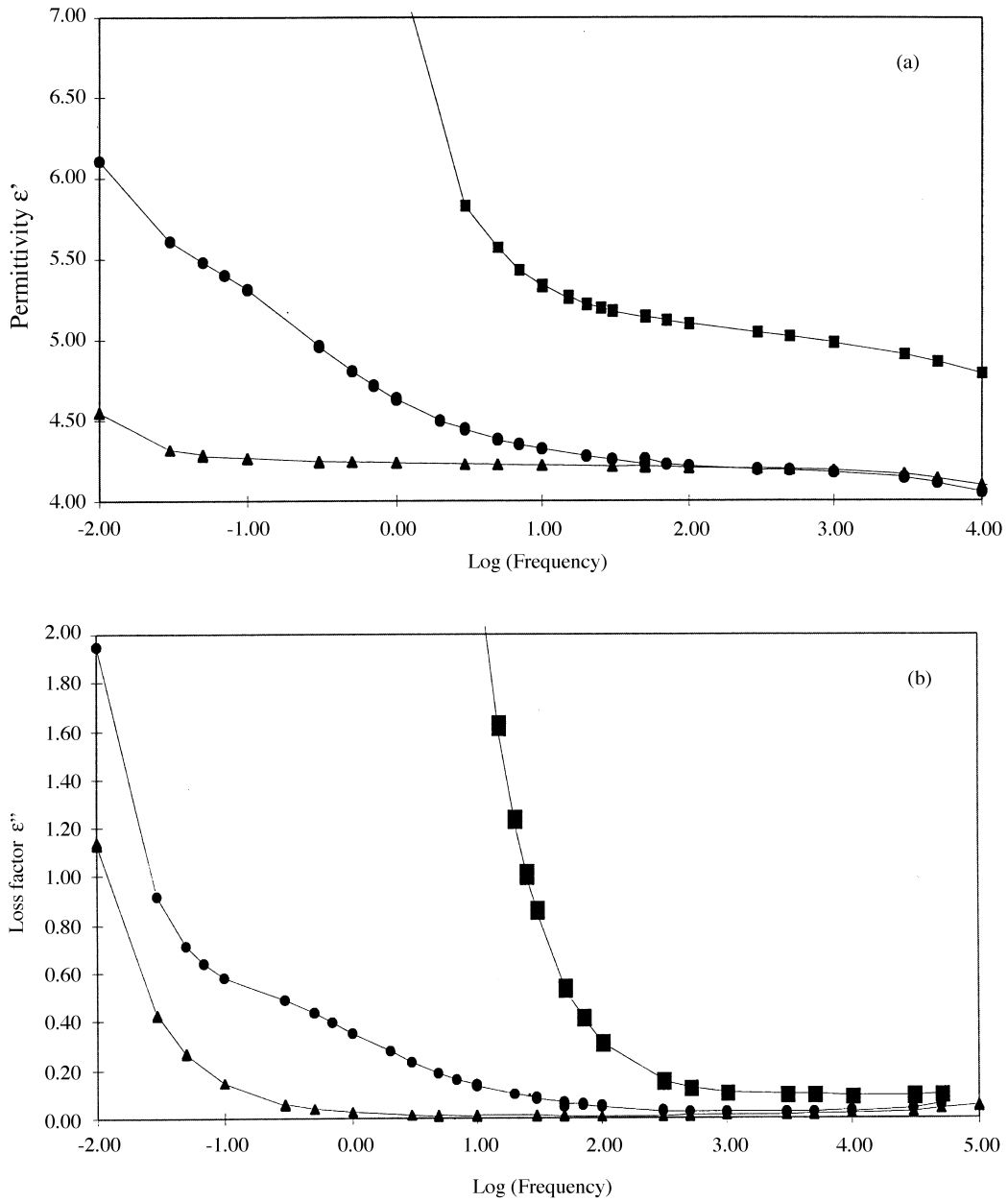

Figure 8 (a) The dielectric constant ε' of the neat epoxy network (▲), CSR1-modified epoxy network (●) and CSR1 film (■) as a function of frequency at 100°C. (b) The loss factor ε'' of the neat epoxy network (▲), CSR1-modified epoxy network (●) and CSR1 film (■) as a function of frequency at 100°C

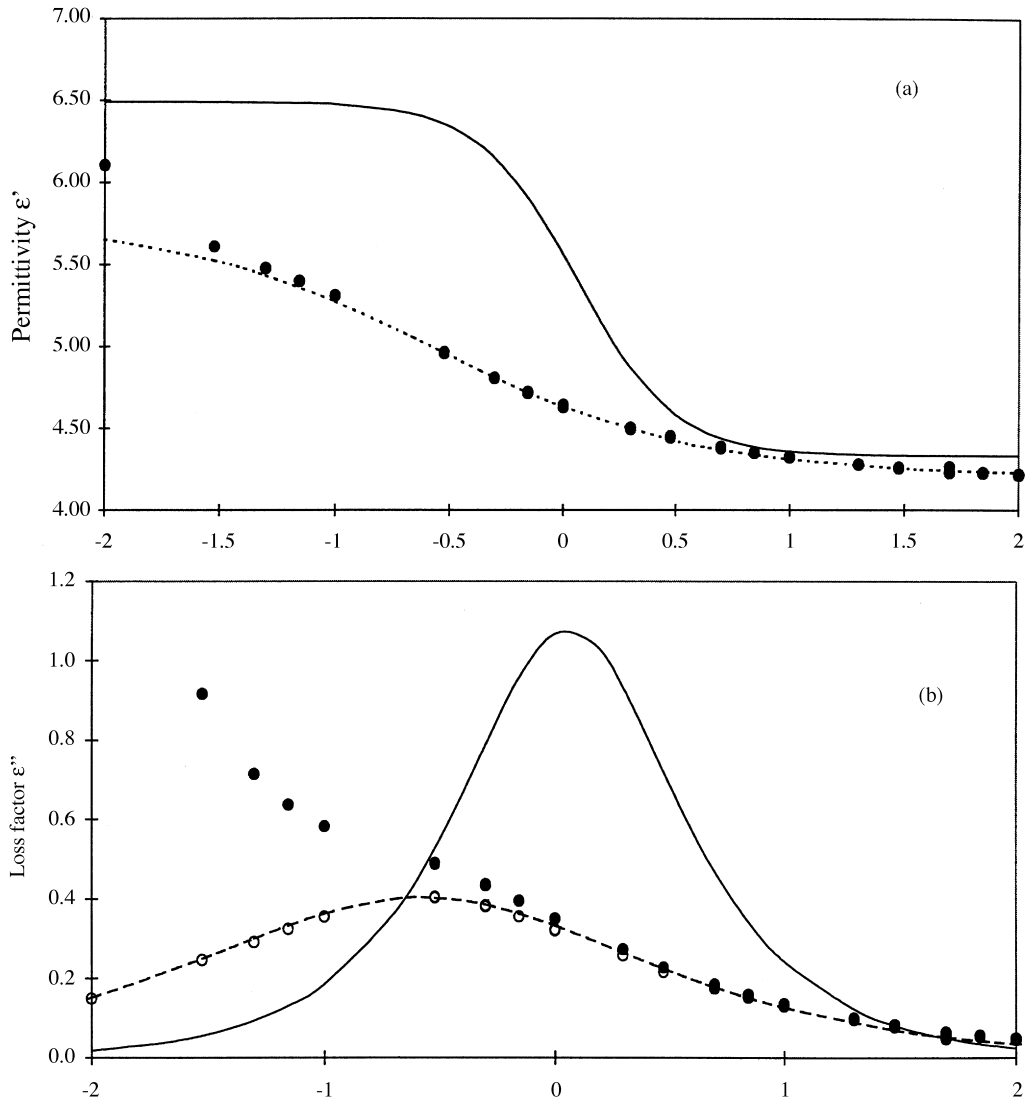

Figure 9 (a) The dielectric constant ε' of CSR1-modified epoxy network (●), the fit with the Cole–Cole equation (dashed lines), and the MWS prediction (full line) at 100°C. (b) The loss factor ε'' of CSR1-modified epoxy network (●), the calculated loss factor ε'' after subtraction of the DC conductivity (○), the fit using the Cole–Cole equation (dashed lines), and the MWS prediction (full line) at 100°C

epoxy network. As mentioned by Pethrick and co-workers[12–14], the shape of the loss curves is very sensitive to the subtraction of the DC conductivity. Too large a subtraction artificially sharpens the peak (by reducing the amplitude at low frequencies), reduces the intensity and increases the position of the maximum on the frequency axis, whereas too small a subtraction leads to the reverse effect. Between the Cole–Cole and the Cole–Davidson equations[5], the only one which allowed us to both fit ε' and ε'' curves was the Cole–Cole formula expressed by

$$\varepsilon^*(\omega) = \varepsilon_\infty + \frac{(\varepsilon_s - \varepsilon_\infty)}{1 + (\mathrm{j}\omega\tau_0)^\beta} \quad 0 \le \beta \le 1 \tag{16}$$

Further, equation (16) can be separated into real and imaginary parts:

$$\frac{\varepsilon'(\omega) - \varepsilon_\infty}{\varepsilon_s - \varepsilon_\infty} = \frac{(1 + (\omega\tau_0)^\beta \cos \beta\pi/2)}{1 + 2(\omega\tau_0)^\beta \cos \beta\pi/2 + (\omega\tau_0)^{2\beta}} \tag{17}$$

$$\frac{\varepsilon''(\omega)}{\varepsilon_s - \varepsilon_\infty} = \frac{(\omega\tau_0)^\beta \sin \beta\pi/2}{1 + 2(\omega\tau_0)^\beta \cos \beta\pi/2 + (\omega\tau_0)^{2\beta}} \tag{18}$$

When $\beta = 1$, equation (16) reduces to the Debye equation. τ_0 is the mean relaxation time and β is a measure of the distribution of relaxation times.

At each temperature, a contribution which varies as in $C(T)/\omega^{0.9}$ was subtracted from the dielectric loss index, with $C(T) = \sigma_{DC}(T)/\varepsilon_0$. C was increased to the upper limit for which the shape of the Cole–Cole plot was that of a symmetric circular arc with its centre lying below the horizontal axis. Above this upper limit an apparent skewed arc was displayed because the amplitude at the low frequencies was too reduced. The maximum observed in the loss factor determined the mean relaxation time. The dielectric increment, $\varepsilon_s - \varepsilon_\infty$, was estimated from the Cole–Cole plots, and the parameter β was calculated, using the following equation[5]:

$$\varepsilon''_{\max} = \frac{\varepsilon_s - \varepsilon_\infty}{2} \tan \beta\pi/4 \tag{19}$$

The resulting subtracted data and the fits at 100°C are plotted in *Figure 9a* and *b*. An Arrhenius temperature dependency as predicted by the MWS model is displayed for the resulting relaxation times (*Figure 10*). The extracted relaxation strength $\varepsilon_s - \varepsilon_\infty$ is found to increase with

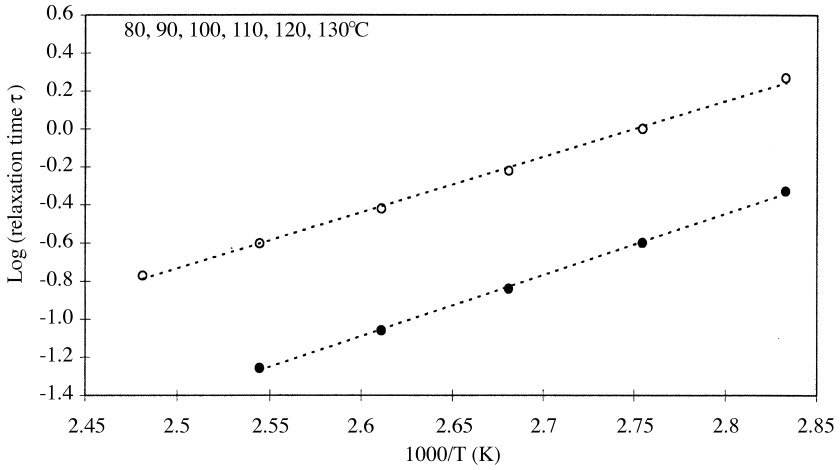

Figure 10 Log (interfacial relaxation time) *versus* (1000/*T*), (●): predicted by the MWS model and (○) extracted from the Cole–Cole analyses for the CSR1-modified epoxy network

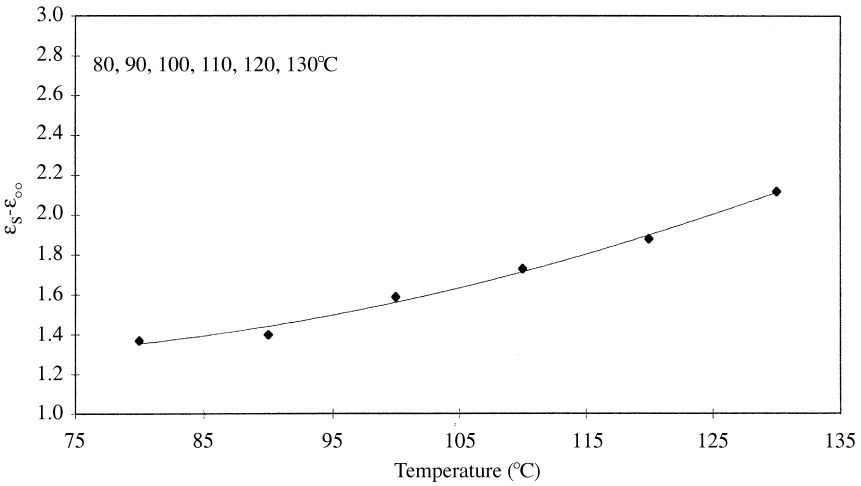

Figure 11 Interfacial relaxation strength $\varepsilon_s - \varepsilon_\infty$ extracted from the Cole–Cole analysis as a function of temperature for the CSR1-modified epoxy network

temperature (*Figure 11*). A mean $\beta = 0.60 \pm 0.02$ value can be estimated.

DISCUSSION

As observed in *Figure 3*, the high conductivity measured for the CSR1 particles can be attributed to the poly(butyl acrylate) core. In the measuring temperature range, i.e. 100–180°C above its T_g, it must be in the form of a highly conductive polar fluid. Given the low polarity of the polybutadiene, such a level of conductivity is not observed for the CSR2 particles. The low conductivity measured for the poly(methyl methacrylate) suggests that we may consider the CSR1 particles as a conductive core surrounded by an insulating shell and the moulded films as conductive spheres occluded in an insulating matrix. However, in such a case, charge carriers would build up at the interface between the core and the shell. Using the conductivities measured between 80 and 120°C on the poly(methyl methacrylate) and on the CSR1 moulded film for σ_1 and σ_2 a huge MWS process is predicted with $\varepsilon_s - \varepsilon_\infty$ reaching 50 in the frequency range from 0.1 to 1 Hz (equations (4)–(6)). Such a phenomena was not displayed in the dielectric spectrums of the CSR1 moulded films. As a result we have to consider the possibility that the poly(methyl methacrylate) shell isn't insulating for the poly(butyl acrylate) charge carriers. This might be due to the shell thickness which is only 7 nm. In polymeric materials like the ones studied here the concept of band conduction by free charge carriers does not apply and charge transport occurs by a hopping mechanism operating between localized sites such as polar or ionic groups[51]. Jumping distances of 8–20 nm have been calculated for poly(ethylene terephtalate) and for polypropylene[52]. This suggests that the shell might be too thin to limit the percolation of charge carriers, which can be concluded from the sharp rise in the loss factor, ε'', due to ohmic electrical conduction just after the glass–rubber transition of the poly(butyl acrylate) core (*Figure 4*) and the insensitivity of the temperature dependency of the measured conductivity to the glass–rubber transition of the poly(methyl methacrylate) shell (*Figure 3*). Thus, predictions have been carried out considering homogeneous particles occluded in an homogeneous matrix. The conductivity measured on the moulded CSR1 film was taken to be σ_2.

For these acrylic spherical core–shell particles of uniform size where orientation is not a parameter of the modeling, the MWS model predicts the relaxation times shown in *Figure 10*. The temperature dependence of the relaxation times both measured and predicted is in good agreement.

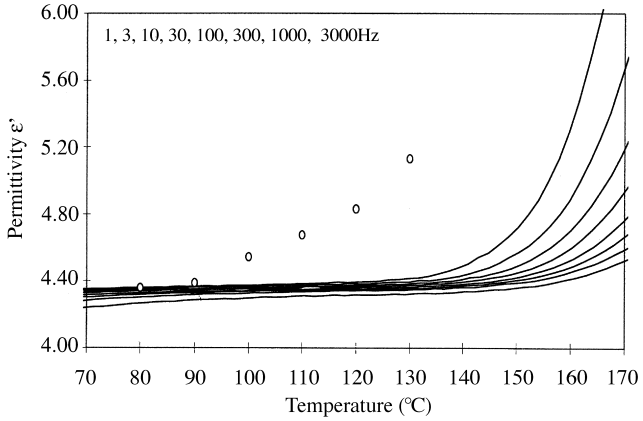

Figure 12 Depiction of the core–shell morphologies in the cured-epoxy network: (a), ideal; (b), real

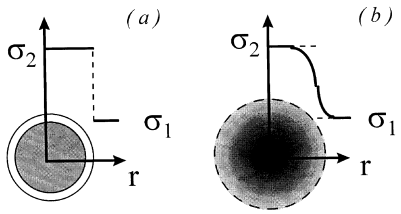

Figure 13 Transition in conductivity at the interface of the core–shell particles in the cured-epoxy network: (a), ideal; (b), real

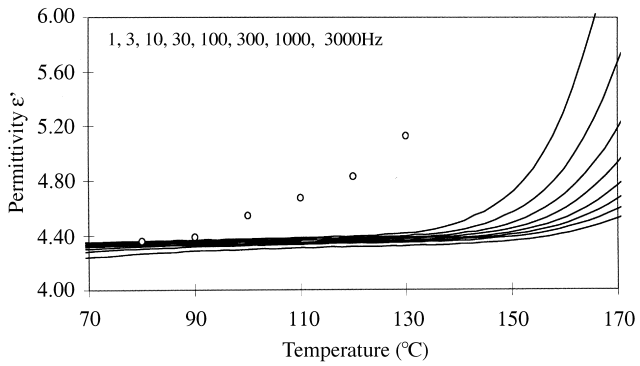

Figure 14 Dielectric constant ε' of unmodified epoxy network (full lines) as a function of temperature at several frequencies and back calculated values of the low frequency ε_{1s} permittivity of the matrix with equation (5) and $\nu_2 = 0.11$ (○)

Clearly the temperature dependence of σ_1 and σ_2 does a good job of predicting the change in τ_{MWS} with temperature.

The predicted values of τ differ by a factor of 4.5. The predicted values using equation (4) are nonsensitive to the volume fraction ν_2 as equation (11) shows. However the predicted values assume that the conductivity, σ_2, of the occluded particles is unchanged from the moulded core–shell film to the particles in the epoxy. This assumption is questionable because the value of σ_1 for the epoxy matrix is increased by a factor of 3.5 from the neat network. Values obtained from DC conductivity measurements are reported *Figure 3*. They were found to correlate well with values of σ_1 used in the subtraction process. Diffusion in the matrix of sodium dodecyl sulfate surfactant initially adsorbed on the particles is likely to occur, which must increase the conductivity of the epoxy phase. However, in order for the predicted absolute value of τ_{MWS} to agree with the measured value, σ_2 would have to be reduced by a factor of 5. As previously mentioned, charge transport can occur by a hopping mechanism. The probability of a hopping transition is determined by the combined effect of the distances between the two sites and the potential barrier that has to be overcome. Thus conductive properties are determined by the most difficult transitions which limit the percolation of charge carriers from one electrode to the other. Associated with a narrow interface between a conductive phase and a less conductive phase is a strong potential barrier where charge carriers are blocked. Shaffer *et al.* have shown that core–shell particles of a poly(butadiene-*co*-styrene) core with slightly reticulated poly(methyl methacrylate-acrylonitrile) shell are swelled by the epoxy prepolymer during the dispersion process[53]. After curing, the final particle morphology is a shell or core–shell with an epoxy gradient concentration. The ideal and real core–shell morphologies in this study are depicted in *Figure 12*. The resulting interface is a diffuse one. Correlation between the hopping probability of charge carriers and molecular mobility of the polymeric environment is easy to envisage. Detrapping from localized sites like strong dipoles or charge transport along the backbone or side groups must be favoured by segmental motions. So, utilizing the concept of a gradient concentration we think that in place of a high potential barrier, numerous weaker ones with larger hopping probabilities are associated with this diffuse interface, which permit the injection of charge carriers from the conductive phase to the less conductive phase. The consequence is that there isn't a sharp transition in conductivity at the interface but a continuous decrease as depicted in *Figure 13*. So, at the interface the difference $\sigma_2 - \sigma_1$, which is considered in equation (4), is reduced and τ_{MWS} is increased.

The high frequency limiting permittivities, $\varepsilon_{1\infty}$ (4.20) and $\varepsilon_{2\infty}$ (4.50), determined from isothermal runs, gave a value of 4.24 for the high frequency limiting permittivity ε_∞ (equation (6)) which is near to the 4.20 measured value. To calculate the low frequency limiting permittivity ε_s (equation (5)), those ε_1 and ε_2 values couldn't be used because the unmodified epoxy network and CSR1 films display a frequency dependent behavior. The lowest measuring frequency available for our equipment, 0.01 Hz, didn't permit a direct measurement of the low frequency limiting permittivities ε_{1s} and ε_{2s}. However, equation (3) can be reduced to equation (20) for small ν_2 and $\sigma_1 \ll \sigma_2$:

$$\varepsilon_s = \varepsilon_{1s}(1 + 3\nu_2) \tag{20}$$

Only ν_2 and ε_{1s} govern the ε_s value.

Shown in *Figure 14* are calculated values of ε_{1s} using equation (5) and the experimental ε_s determined at the low frequency end of the Cole–Cole dispersion. Unlike the prediction of τ_{MWS}, equation (3) is quite sensitive to the value of ν_2. The best fit back calculated values of ε_{1s} occurred when the volume fraction of occluded conducting particles is set to 0.11. This result might reflect the extent of swelling of the particles by the epoxy network. Given the volume fraction of the core–shell particles and the shell thickness, the volume fraction of the poly(butyl-acrylate) core is 0.13; or it suggests that the MWS model is not reliable to accurately predict the interfacial polarization intensity when diffused interfaces are considered.

The low frequency limiting permittivities ε_{1s} increase with temperature. We believe it is a consequence of a low frequency polarization process in the matrix. This assumption is supported by recent work by Wu and Tung[54]. They showed that the oscillating motions of charge carriers under an alternative electrical field lead to a low-frequency relaxation behaviour. For an epoxy network based on a prepolymer DGEBA and nadic methyl anhydride, the

characteristic frequencies are between 10^{-6} and 10^{-4} Hz at temperatures between 10 and 40°C. The frequency behaviour of the neat epoxy network shown in *Figure 14* and the shape of the low frequency limiting permittivity ε_{1s} curve suggest that the lower frequency involved in the interfacial polarization process is 10^{-4} Hz.

The Cole–Cole distribution factor β, that gave the best fit to the dielectric data for the epoxy-core–shell particle system, was 0.6. The MWS model predicts a Debye-like relaxation for spherical particles of uniform composition. Thus a value of β equal to 1 is predicted by the MWS model. It is interesting to speculate why there is a relatively broad distribution of relaxation times. We propose that the distribution in τ for this very uniform spherical dispersion of core–shell particles can arise at the interface, a narrow one leading to a narrow spatial distribution of charge carriers, and a large one leading to a large spatial distribution of charge carriers trapped in the interfacial zone.

CONCLUSIONS

For this blend of polymer materials based on acrylic spherical core–shell particles of uniform size dispersed in an epoxy network, where orientation is not a parameter of the modeling, the MWS model does appear to provide accurate predictions of the dielectrical properties ε_1, ε_2 and σ_2 temperature dependence of τ_{MWS}, the relaxation time of the interfacial polarization process. For a sharp interface, the MWS model predicts a single relaxation time with $\beta = 1$ for the Cole–Cole parameter. A value of $\beta = 0.6$ provided the best fit to this system of uniform spherical particles. This distribution in relaxation time is attributed to a gradient in concentration across the interface, a phenomena which is likely to occur during the formation of many two-phase polymer systems. Thus the main additional modification needed for the MWS model is the ability to predict the distribution in relaxation times as measured by a parameter such as the Cole–Cole distribution factor β based on the nature of the interface and the details of charge transfer. The nature and properties of interphases should strongly influence the dielectrical properties and interfacial polarization processes in polymer blends, and might lead to an erroneous description of the morphologies through the use of theoretical models which do not recognize the need to include the physical and chemical nature of the interface. Overall, the results suggest that dielectric spectroscopy can be a high sensitivity technique to study the interfacial characteristics in polymer blends such as the degree of inter-diffusion.

ACKNOWLEDGEMENTS

David E. Kranbuehl appreciates partial support form the NSF Science and Technology Center at Virginia Polytechnic Institute and State University under Contract #DMR91-2004, a NASA Langley grant NAG1-23.

REFERENCES

1. Kranbuehl, D., *Developments in Reinforced Plastics*, Vol. 5. Elsevier Applied Science, New York, 1986, pp. 181–204.
2. Kranbuehl, D., in *Encyclopedia of Composites*, ed. Stuart M. Lee. VCH Publishers, New York, 1989, pp. 531–43.
3. Senturia, S. and Sheppard, S., *J. Appl. Polym. Sci.*, 1986, **80**, 1.
4. May, C., Chemorheology of Thermosetting Resins, in *Polymer Materials Science and Engineering*, ACS Symposium Series 227. American Chemical Society, Washington, DC, 1983.
5. Hedvig, P., *Dielectric Spectroscopy of Polymers*. Wiley, New York, 1977.
6. Mijovic, J. and Winnie Tee, C. F., *Macromolecules*, 1994, **27**, 7287.
7. Parthum, M. B. and Johari, G., *Macromolecules*, 1992, **25**, 3254.
8. Mathieu, C., Boiteux, G., Seytre, G., Villain, R. and Dublineau, P., *J. Non-Crystalline Solids*, 1994, **172**, 1012.
9. Deng, Y. and Martin, G., *Macromolecules*, 1994, **27**, 5141.
10. Companik, J. and Bidstrup, S., *Polymer*, 1994, **35**, 4823.
11. Brown, J. M., Srinivasan, S., Ward, T., McGrath, J., Loos, A. C., Hood, D. and Kranbuehl, D., *Polymer*, 1996, **37**, 1691.
12. MacKinnon, A. J., Jenkins, S. D., MacGrail, P. T. and Pethrick, R. A., *Polymer*, 1993, **34**, 3252.
13. MacKinnon, A. J., Jenkins, S. D., MacGrail, P. T. and Pethrick, R. A., *Macromolecules*, 1992, **25**, 3492.
14. Delides, C. G., Hayward, D., Pethrick, A. and Vatalis, A. S., *Europ. Polym. J.*, 1992, **28**, 505.
15. Maistros, G., Block, H., Bucknall, C. B. and Partridge, I. K., *Polymer*, 1992, **33**, 4470.
16. Korkakas, G., Gomez, C. M. and Bucknall, C. B., *Plastic Rubbers Composites Processing and Applications*, 1993, **19**, 285.
17. Kranbuehl, D., Kim, T., Liptak, S. C. and McGrath, J. E., *Polymer Preprints*, 1993, **34**, 488.
18. Van Beek, L. H. K., *Progress in Dielectrics*, 1967, **7**, 69.
19. Bánhegyi, G., *Colloïd & Polym. Sci.*, 1986, **264**, 1030.
20. Bánhegyi, G., *Colloïd & Polym. Sci.*, 1986, **266**, 11.
21. Maxwell, J. C., *Electricity and Magnetism*, Vol. 1. Clarendon, Oxford, 1892.
22. Wagner, K. W., *Arch. Electotech.*, 1914, **2**, 378.
23. Sillars, R. W., *J. Inst. Electr. Eng.*, 1937, **80**, 378.
24. Fricke, H., *J. Phys. Chem.*, 1953, **57**, 934.
25. Hanaï, T., *Emulsion Science*, ed. P. Sherman. Academic Press, New York, London, 1968, p. 353.
26. Boyle, M. H., *Colloïd & Polym. Sci.*, 1985, **263**, 51.
27. Boned, C. and Peyrelasse, J., *Colloïd & Polym. Sci.*, 1983, **261**, 600.
28. Steeman, P. A. M. and Maurer, F. H. J., *Colloïd & Polym. Sci.*, 1990, **268**, 315.
29. Steeman, P. A. M. and Maurer, F. H. J., *Colloïd & Polym. Sci.*, 1990, **270**, 1069.
30. Looyenga, H., *Physica*, 1965, **31**, 401.
31. Böttcher, C. J. F., *Rec. Trav. Chim.*, 1945, **64**, 47.
32. Hsu, W. Y., Gierke, T. D. and Molnar, J. C., *Macromolecules*, 1983, **16**, 1945.
33. Daly, J. H., Guest, M. J., Hayward, D. and Pethrick, R. A., *J. Mater. Sci. Letters*, 1992, **11**, 1271.
34. Suthar, B., Klempner, D., Frisch, K. C., Petrovic, Z. and Jelcic, Z., *J. Appl. Polym. Sci.*, 1994, **53**, 1083.
35. Sreehari Sasstry, S., Satyanandam, G., Sundar Raj, T. F. and Vasanthakumari, R., *J. Appl. Polym. Sci.*, 1988, **36**, 1607.
36. La Mantia, F. P., Schifani, R. and Acierno, D., *J. Appl. Polym. Sci.*, 1983, **28**, 3075.
37. Bánhegyi, G., Szaplonczay, P., Frojimovics, G. and Karasz, F. E., *Polym. Composites*, 1990, **11**, 133.
38. Bánhegyi, G., Rho, M.-K., Chien, J. C. W. and Karasz, F. E., *J. Polym. Sci.: Part B: Polym. Phys. Ed.*, 1987, **25**, 57.
39. LaMantia, F. P., Valenza, A. and Acierno, D., *Colloïd & Polym. Sci.*, 1985, **263**, 726.
40. Pratt, G. J. and Smith, M. J. A., *Polymer*, 1989, **30**, 1113.
41. Pillai, P. K. C., Gupta, B. K. and Goel, M., *J. Polym. Sci.: Part B.: Polym. Phys. Ed.*, 1981, **19**, 1461.
42. Rellinck, G. S. and Runt, J., *J. Polym. Sci.: Part B: Polym. Phys. Ed.*, 1988, **26**, 1425.
43. Eklind, H., Maurer, F. H. J. and Steeman, P. A. M., *Polymer*, 1997, **38**, 1047.
44. Jeffery, A.-M. and Damon, D. H., *IEEE Transactions on Dielectric and Electrical Insulation*, 1995, **2**, 394.
45. Perrier, G. and Bergeret, A., *J. Appl. Phys.*, 1995, **77**(6), 1.
46. Steeman, P. A. M., Maurer, F. H. J. and Van Turnhout, J., *Polym. Engi. Sci.*, 1994, **34**, 697.
47. Aldrich, P. D., McGee, R. L., Yalvac, S., Bonehamg, J. E. and Thurow, S. W., *J. Appl. Phys.*, 1987, **62**, 6504.
48. Steeman, P. A. M., Gondard, C. and Scherrenberg, L., *J. Polym. Sci.: Part B: Polym. Phys.*, 1984, **32**, 119.
49. Lu, M. and Paul, R. R., *Polymer*, 1996, **37**, 115.
50. Mangion, B. B. R. and Johari, G. P., *Macromolecules*, 1990, **23**, 3687.
51. Jonscher, A. K., *Dielectric Relaxation in Solids*. Chelsea Dielectrics Press, London, 1982.
52. Seanor, D. A., *Electrical Properties of Polymers*. Academic Press, New York, 1982, pp. 1–55.
53. Shaffer, O. L., Bagheri, R., Qian, J. Y., Dimonie, V., Pearson, R. A. and El- Aasser, M. S., *J. Appl. Sci.*, 1995, **58**, 465.
54. Wu, S. L. and Tung, I. C., *J. Mater. Sci.*, 1996, **31**, 2177.